Iranian Journal of
Numerical Analysis and Optimization

Ferdowsi University of Mashhad

Reaserch Article

Mathematical analysis of Mpox transmission using an SAIR-SI model with optimal control strategies

T. Janan, F. Fatmawati and A. Hasan

DOI:10.22067/ijnao.2026.100294.1934

Vol. 17, No. 1, March 2027

pp. 380–415

Ferdowsi University of Mashhad, Iran

Iranian Journal of Numerical Analysis and Optimization
Vol. 17, No. 1, 2027, pp 380–415
https://doi.org/10.22067/ijnao.2026.100294.1934
https://ijnao.um.ac.ir/

CC BY NC

Research Article

Mathematical analysis of Mpox transmission using an SAIR-SI model with optimal control strategies

T. Janan, F. Fatmawati*, and A. Hasan

Abstract

This study presents an SAIR-SI (susceptible-asymptomatic-symptomatic-recovered-susceptible-infected) mathematical model of Mpox transmission using real data from the United States. First, the well-posedness, boundedness, and nonnegativity of the solutions are analyzed. Then, it is shown that the model admits three equilibria: Disease-free, human-endemic, and endemic. The local stability of the disease-free equilibrium is analyzed based on the Jacobian matrix, while the global stability of all equilibria is examined by defining distinct Lyapunov functions. Sensitivity analysis highlights transmission strength and progression rate as major determinants of epidemic behavior. Numerical simulations demonstrate that higher transmission

*Corresponding author

Received 6 August 2026; revised 9 September 2026; accepted 19 September 2026

Tuhfatul Janan
Department of Mathematics, Faculty of Science and Technology, Universitas Airlangga, Surabaya, Indonesia. e-mail: tuhfatuljanan1@gmail.com. Department of Mathematics Education, Faculty of Education and Teacher Training, Institut Ahmad Dahlan Probolinggo, Probolinggo, Indonesia

Fatmawati Fatmawati
Department of Mathematics, Faculty of Science and Technology, Universitas Airlangga, Surabaya, Indonesia. e-mail: fatmawati@fst.unair.ac.id

Agus Hasan
Department of ICT and Natural Sciences, Norwegian University of Science and Technology, Alesund, Norway. e-mail: agus.hasan@ntnu.no

How to cite this article
Janan, T., Fatmawati, F. and Hasan, A., Mathematical analysis of Mpox transmission using an SAIR-SI model with optimal control strategies. *Iran. J. Numer. Anal. Optim.*, 2027; 17(1): 380-415. https://doi.org/10.22067/ijnao.2026.100294.1934

accelerates spread, while slower progression from asymptomatic to symptomatic stages prolongs infectiousness and increases disease burden. Furthermore, two control measures, namely vaccination and rodenticide usage, are considered, and the optimal control problem is formulated based on Pontryagin's principle. Numerical simulations incorporating control measures demonstrate that the strategy combining both controls is the most effective approach for reducing the asymptomatic human, symptomatic human, and infected rodent subpopulations. The cost-effectiveness analysis also confirms that the combined implementation of vaccination and rodenticide usage is the most efficient strategy.

AMS subject classifications (2020): 37N25, 49K40, 92-10, 92B05, 93-10.

Keywords: Mpox disease: Asymptomatic humans; SAIR-SI model; Stability analysis; Optimal control.

1 Introduction

Monkeypox (Mpox) is a zoonotic disease caused by the Mpox virus, a member of the Orthopoxvirus genus, which is phylogenetically related to the variola virus [10]. The virus is classified into two major clades, namely Clade I (subclades Ia and Ib) and Clade II (subclades IIa and IIb). The first case was identified in monkeys in Denmark in 1958, while human infection was first reported in the Democratic Republic of Congo in 1970 [35]. Although Mpox remains endemic in several African regions, since May 2022 its transmission has expanded to nonendemic countries, primarily linked to international travel to Europe and North America [34]. With the rapid global increase in cases, the World Health Organization (WHO) declared Mpox a Public Health Emergency of International Concern on August 14, 2024, after more than 100,000 cases and 220 deaths had been reported across 120 countries [37].

Transmission occurs through direct contact with infected individuals, animal reservoirs, or contaminated objects [12]. Routes of infection include respiratory droplets, skin lesions, body fluids [28], and possible vertical transmission from mother to fetus or newborn [38]. In zoonotic contexts, transmission may occur through bites or contact with fluids of infected animals, such as during hunting or consumption of bushmeat [35, 12, 2]. Fomite transmission via contaminated materials such as clothing and bedding has also been documented [12]. The incubation period of Mpox is generally from 6 to 13 days but can range from 5 to 21 days [30, 31]. During this period, infected individuals remain asymptomatic and clinically well. Typical clinical manifestations include rash, fever, sore throat, headache, myalgia, back pain, fatigue, and lymphadenopathy. Most symptoms will last for approximately 2–4 weeks. With good supportive care, the vast

majority of cases will improve. Severe outcomes and mortality are most likely in newborns, children, pregnant women, and immunocompromised patients, including patients in the advanced stages of HIV infection. According to the WHO, the case fatality ratio ranges from 0.1% to 10% [36].

With several hundred cases developing daily, the United States (U.S.) is currently one of the countries most affected by the recent Mpox outbreaks, which occurred between July and September 2022 [13]. The Department of Health and Human Services distributed over one million vials of the JYNNEOS vaccine nationwide from August 2022 to August 2024, in an effort to reduce transmission and the severity of this disease [11]. Governmental efforts have also aimed at promoting research into Mpox, concentrating on viral mechanisms for transmission, host immune responses, and optimization of vaccine dosing regimens to increase supply and facilitate new vaccine development. In addition to vaccination strategies, therapeutic interventions involving the use of antivirals and monoclonal antibodies, along with laboratory diagnostic system strengthening, remain crucial for patient management and epidemiological surveillance [32].

Mathematical modeling has been consistently used as a tool for understanding infectious disease dynamics and formulating control strategies effectively [26, 27]. The classical compartmental model, which classifies the population into susceptible, infected, and recovered subpopulations, is the bedrock of other more developed epidemiological models [15, 18, 40]. In recent times, there has been the inclusion of extra compartments such as vaccinated [3, 33] and asymptomatic [1, 29] status to give these models real-world representation in public health contexts. This extension has greatly improved the ability of the models to assess the effectiveness of intervention measures. For example, Al-Shomrani, Musa, and Yusuf [7] illustrated that the inclusion of extra subpopulations leads to more accurate estimation of policy impacts.

In the case of Mpox, the transmission models generally consider interactions between the human and rodent populations. Thus, Alshehri and Ullah [6] presented a framework that divided the human subpopulations into susceptible, infected, quarantined, and recovered groups while dividing the rodent population into two classes of susceptible and infected populations. Based on this, the extension introduced by Allehiany et al. [4] further extended the classes by incorporating exposed compartments for humans and rodents. Further refinements were made by Wireko et al. [39], who integrated an isolation compartment into the human model creating six categories: Susceptible, exposed, infected, isolated, quarantined, and recovered. In the refinement to the rodents, Yapışkan et al. [41] incorporated a recovered subpopulation into the standard susceptible-infected structure, while Al-Shomrani, Musa, and Yusuf [7] further extended this by incorporating an exposed class.

The WHO also emphasized that asymptomatic individuals with Mpox virus infection can still transmit the disease in the absence of symptoms and clinical signs [35]. Li et al. [24] have ex-

plicitly modeled asymptomatic individuals to realistically capture the dynamics of transmission. According to their analysis, the asymptomatic group is crucial in sustaining chains of infection. This calls for prioritizing asymptomatic carriers with intervention measures such as vaccination and personal protection. Likewise, Fernandes and Maldonado [17] demonstrated that asymptomatic carriers can be capable of spread the virus via sexual contact, hence their relevance in determining the probabilities of transmission. These findings are of great importance to public health authorities in developing prevention policies, particularly those dealing with sexually transmitted infections with latent or asymptomatic routes of transmission. Additional studies related to Mpox modeling can be found in [8, 20, 22, 25, 42].

It is against this backdrop that this study presents an SAIR-SI mathematical model for Mpox transmission in the United States, which explicitly includes asymptomatic humans. In developing the model, recent evidence has been used to highlight the critical role played by asymptomatic individuals in disease transmission, which previous models have often ignored. The proposed model is subsequently extended by incorporating an optimal control framework to further investigate effective control strategies for suppressing the spread of Mpox. In this extended model, two control measures are considered, namely vaccination and rodenticide usage, which are evaluated using Pontryagin's principle. Each control strategy is systematically illustrated through comparison with the uncontrolled scenario in order to assess its effectiveness in reducing the asymptomatic human, symptomatic human, and infected rodent subpopulations. Overall, compared with previous Mpox transmission models that incorporate asymptomatic individuals, this study extends the existing framework by using data from the United States in 2022, considering vaccination and rodenticide usage as control measures, and evaluating their cost-effectiveness using the ICER method, as summarized in Table 1.

Table 1: Comparison of recent Mpox transmission models

Reference	Data	Control measures	Cost-effectiveness
[7]	Nigeria, 2022	None	None
[17]	Multiple countries	None	None
[24]	Nigeria, 2022-2023	Personal protection, vaccination, and reduced animal contact	None
This study	United States, 2022	Vaccination and rodenticide usage	ICER method

2 Mathematical model and basic properties

2.1 Mathematical model

The SAIR-SI mathematical model explicitly captures the transmission dynamics of Mpox, incorporating interactions between human and rodent populations. The human host population is stratified into four epidemiological compartments: susceptible humans (S_h), asymptomatic humans (A_h), symptomatic infected humans (I_h), and recovered humans (R_h). In contrast, the rodent population is structured into two classes: Susceptible rodents (S_r) and infected rodents (I_r). The total human population at any time is expressed as $N_h = S_h + A_h + I_h + R_h$, while the total rodent population is represented as $N_r = S_r + I_r$. The transmission diagram of Mpox dynamics is illustrated in Figure 1.

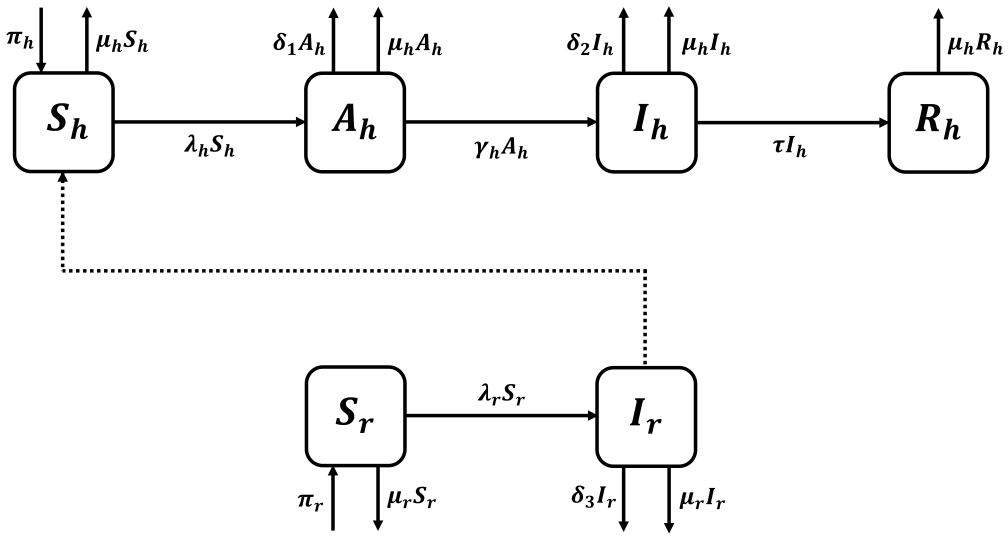

Figure 1: Mpox transmission diagram

Within the human host population, the pool of susceptible humans grows through recruitment at a constant rate (π_h). These individuals are subject to infection either through effective contact with asymptomatic humans, symptomatic infected humans, or infectious rodents, and may also be lost due to natural mortality at rate μ_h. The risk of infection in humans is characterized by the force of infection, $\lambda_h = \frac{\beta_1 A_h + \beta_2 I_h + \beta_3 I_r}{N_h}$, where β_1, β_2, and β_3 represent the respective effective contact rates with asymptomatic humans, symptomatic humans, and infected rodents.

Asymptomatic humans, despite not showing clinical manifestations, remain infectious and thus contribute to onward transmission. They may transition to the symptomatic class at rate γ_h or be removed from the population due to Mpox-induced mortality (δ_1) or natural causes (μ_h). Symptomatic individuals can either recover at rate τ or experience disease-induced death (δ_2) and natural death (μ_h). In the rodent reservoir population, susceptible rodents enter the system at a recruitment rate (π_r) and are exposed to infection through effective contact with infectious rodents, governed by the force of infection $\lambda_r = \frac{\beta_4 I_r}{N_r}$, with β_4 denoting the effective contact rate. Both susceptible and infected rodents are subject to natural mortality (μ_r), whereas infected rodents additionally face Mpox-induced mortality at rate δ_3. A detailed description of each parameter is provided in Table 2.

Table 2: Description of parameters

Parameter	Description
π_h	Rate of entry of susceptible humans
π_r	Rate of entry of susceptible rodents
β_1	Transmission rate via contact with asymptomatic humans
β_2	Transmission rate via contact with symptomatic humans
β_3	Transmission rate from infected rodents to humans
β_4	Transmission rate among rodents
γ_h	Rate of progression from asymptomatic to symptomatic infection in humans
τ	Recovery rate of symptomatic humans
δ_1	Mpox-induced death rate in asymptomatic humans
δ_2	Mpox-induced death rate in symptomatic humans
δ_3	Mpox-induced death rate in rodents
μ_h	Natural death rate of humans
μ_r	Natural death rate of rodents

The dynamics of Mpox transmission are mathematically described using the following system of differential equations:

$$\begin{aligned}
\frac{dS_h}{dt} &= \pi_h - (\lambda_h + \mu_h)S_h, \\
\frac{dA_h}{dt} &= \lambda_h S_h - (\gamma_h + \delta_1 + \mu_h)A_h, \\
\frac{dI_h}{dt} &= \gamma_h A_h - (\tau + \delta_2 + \mu_h)I_h, \\
\frac{dR_h}{dt} &= \tau I_h - \mu_h R_h, \\
\frac{dS_r}{dt} &= \pi_r - (\lambda_r + \mu_r)S_r, \\
\frac{dI_r}{dt} &= \lambda_r S_r - (\delta_3 + \mu_r)I_r,
\end{aligned} \tag{1}$$

with the initial conditions $S_h(0) > 0$, $A_h(0) \geq 0$, $I_h(0) \geq 0$, $R_h(0) \geq 0$, $S_r(0) > 0$, and $I_r(0) \geq 0$.

2.2 Well-posedness analysis

We begin by establishing the well-posedness of model (1) through the application of the contraction mapping theorem, aligning with the methodological framework presented by Elsonbaty et al. [16]. A model is said to be well-posed if its solution satisfies three key criteria: Existence, uniqueness, and continuous dependence on initial conditions (stability). We consider the first differential equation of model (1), expressed as

$$\frac{dS_h}{dt} = \pi_h - (\lambda_h + \mu_h)S_h.$$

Integrating both sides yields the corresponding integral representation:

$$S_h(t) = S_h(0) + \int_0^t (\pi_h - (\lambda_h + \mu_h)S_h)\, ds.$$

Define the operator T acting on S_h by

$$T(S_h(t)) = S_h(0) + \int_0^t (\pi_h - (\lambda_h + \mu_h)S_h)\, ds.$$

Let Y denote a complete metric space defined as

$$Y = \{S_h : [0, a] \to \mathbb{R} \mid S_h \text{ is continuous}\},$$

with the supremum norm,

$$d(S_{h1}, S_{h2}) = \|S_{h1} - S_{h2}\|_\infty = \sup_{t\in[0,a]} |S_{h1}(t) - S_{h2}(t)|.$$

For any $S_{h_1}, S_{h_2} \in Y$, the following inequality holds:

$$\begin{aligned} \left|T(S_{h_1}(t)) - T(S_{h_2}(t))\right| &= \left|\int_0^t -(\lambda_h + \mu_h)\,(S_{h_1} - S_{h_2})\, ds\right| \\ &\leq Ct\,\|S_{h_1} - S_{h_2}\|_\infty, \end{aligned}$$

where $C = \sup_{s\in[0,a]} (\lambda_h + \mu_h)$.
Thus,

$$\|T(S_{h1}) - T(S_{h2})\|_\infty \leq Ca\|S_{h1} - S_{h2}\|_\infty. \tag{2}$$

Therefore, the operator T is a contraction provided that $Ca < 1$, or equivalently $a < \frac{1}{C}$. According to the contraction mapping principle, under this condition there exists a unique fixed point $S_h(t) \in Y$ such that $S_h(t) = T(S_h(t))$.

To investigate the stability of the solution, consider two solutions $S_{h1}(t)$ and $S_{h2}(t)$ with distinct initial values. The corresponding integral forms are

$$S_{h1}(t) = S_{h1}(0) + \int_0^t (\pi_h - (\lambda_h + \mu_h)S_{h1}(s))\, ds,$$
$$S_{h2}(t) = S_{h2}(0) + \int_0^t (\pi_h - (\lambda_h + \mu_h)S_{h2}(s))\, ds.$$

Subtracting and estimating the difference yields

$$\|S_{h_1}(t) - S_{h_2}(t)\|_\infty \leq \|S_{h_1}(0) - S_{h_2}(0)\|_\infty + Ca\, \|S_{h_1} - S_{h_2}\|_\infty,$$

or equivalently,

$$(1 - Ca)\, \|S_{h_1}(t) - S_{h_2}(t)\|_\infty \leq \|S_{h_1}(0) - S_{h_2}(0)\|_\infty.$$

Assuming $0 < \|S_{h1}(0) - S_{h2}(0)\|_\infty \leq \theta$, it follows that

$$0 < \|S_{h1}(t) - S_{h2}(t)\|_\infty \leq \frac{\theta}{1 - Ca} = \varepsilon, \tag{3}$$

where $Ca < 1$ and $C = \sup_{s\in[0,a]}(\lambda_h + \mu_h)$.
This confirms the stability of the solution $S_h(t) \in Y$.

Following similar reasoning, one can show that all other state variables, namely $A_h(t)$, $I_h(t)$, $R_h(t)$, $S_r(t)$, and $I_r(t)$, also satisfy the conditions for existence, uniqueness, and stability. Hence, we conclude that model (1) is well-posed.

2.3 Boundedness and nonnegativity

We now investigate the boundedness of the model's solutions. For the human population, we have

$$\frac{dN_h}{dt} = \pi_h - \mu_h N_h - \delta_1 A_h - \delta_2 I_h \leq \pi_h - \mu_h N_h. \tag{4}$$

Solving this differential inequality leads to

$$N_h(t) \leq \frac{\pi_h}{\mu_h} + \left(N_h(0) - \frac{\pi_h}{\mu_h}\right) e^{-\mu_h t}.$$

Thus,

$$\lim_{t\to\infty} N_h(t) \leq \frac{\pi_h}{\mu_h}. \tag{5}$$

Similarly, for the rodent population, we get

$$\frac{dN_r}{dt} = \pi_r - \mu_r N_r - \delta_3 I_r \leq \pi_r - \mu_r N_r. \tag{6}$$

Solving this differential inequality yields

$$N_r(t) \leq \frac{\pi_r}{\mu_r} + \left(N_r(0) - \frac{\pi_r}{\mu_r}\right) e^{-\mu_r t},$$

implying

$$\lim_{t\to\infty} N_r(t) \leq \frac{\pi_r}{\mu_r}. \tag{7}$$

Hence, all solutions remain bounded within the biologically feasible region:

$$\Omega = \left\{(S_h, A_h, I_h, R_h, S_r, I_r) \in \mathbb{R}^6_+ \mid N_h \leq \frac{\pi_h}{\mu_h},\ N_r \leq \frac{\pi_r}{\mu_r}\right\}. \tag{8}$$

Next, we proceed to verify the nonnegativity of the solutions of model (1), as formally stated in Theorem 1.

Theorem 1. Let $S_h(t), A_h(t), I_h(t), R_h(t), S_r(t)$, and $I_r(t)$ denote the solutions of model (1). If the initial values are nonnegative, then each solution remains nonnegative for all $t \geq 0$.

Proof. Consider the first differential equation of model (1):

$$\frac{dS_h}{dt} = \pi_h - (\lambda_h + \mu_h) S_h.$$

Multiplying both sides by the integrating factor $e^{\mu_h t + \int_0^t \lambda_h\, ds}$ yields

$$\frac{d}{dt}\left(e^{\mu_h t + \int_0^t \lambda_h\, ds} S_h\right) = \pi_h e^{\mu_h t + \int_0^t \lambda_h\, ds}.$$

Solving this equation, we obtain

$$S_h(t) = \left(\int_0^t \pi_h e^{\mu_h y + \int_0^y \lambda_h \, ds} dy + S_h(0) \right) e^{-\mu_h t - \int_0^t \lambda_h \, ds} \geq 0. \tag{9}$$

Since both the exponential term and the integrand are nonnegative, and $S_h(0) \geq 0$, it follows that $S_h(t) \geq 0$ for all $t \geq 0$. Applying analogous steps to the remaining differential equations confirms that the other state variables $A_h(t), I_h(t), R_h(t), S_r(t), I_r(t)$ also remain nonnegative for all $t \geq 0$, provided their respective initial conditions are nonnegative. □

3 Equilibrium and stability analysis

3.1 Equilibrium and basic reproduction number

In this section, we investigate the equilibrium states of model (1) by setting the time derivatives of all state variables to zero, as outlined in [9]. This yields the steady-state conditions

$$\frac{dS_h}{dt} = \frac{dA_h}{dt} = \frac{dI_h}{dt} = \frac{dR_h}{dt} = \frac{dS_r}{dt} = \frac{dI_r}{dt} = 0.$$

Under these conditions, model (1) reduces to the following system of algebraic equations:

$$\begin{aligned} \pi_h - (\lambda_h + \mu_h) S_h &= 0, \\ \lambda_h S_h - m_1 A_h &= 0, \\ \gamma_h A_h - m_2 I_h &= 0, \\ \tau I_h - \mu_h R_h &= 0, \\ \pi_r - (\lambda_r + \mu_r) S_r &= 0, \\ \lambda_r S_r - m_3 I_r &= 0, \end{aligned} \tag{10}$$

where m_1, m_2, m_3 are defined as $m_1 = \gamma_h + \delta_1 + \mu_h, m_2 = \tau + \delta_2 + \mu_h$, and $m_3 = \delta_3 + \mu_r$. The disease-free equilibrium (DFE) corresponds to a scenario in which there is no active Mpox infection in either the human or rodent populations, that is, $A_h = I_h = I_r = 0$. Thus, the DFE of model (1) is given by

$$X^0 = (S_h^0, A_h^0, I_h^0, R_h^0, S_r^0, I_r^0) = \left(\frac{\pi_h}{\mu_h}, 0, 0, 0, \frac{\pi_r}{\mu_r}, 0 \right). \tag{11}$$

We now proceed to derive the basic reproduction number, denoted by $\mathcal{R}_0$, which quantifies the average number of secondary infections generated by a single infectious individual in a fully

susceptible population. In this study, $\mathcal{R}_0$ is computed using the next-generation matrix (NGM) approach. The infected compartments in model (1) are A_h, I_h, and I_r. Focusing on their dynamics, the infected subsystem can be written as

$$\begin{pmatrix} \frac{dA_h}{dt} \\ \frac{dI_h}{dt} \\ \frac{dI_r}{dt} \end{pmatrix} = \begin{pmatrix} \lambda_h S_h \\ 0 \\ \lambda_r S_r \end{pmatrix} - \begin{pmatrix} m_1 A_h \\ -\gamma_h A_h + m_2 I_h \\ m_3 I_r \end{pmatrix}. \tag{12}$$

Linearizing system (12) around the DFE leads to the construction of the Jacobian matrices F and V, representing new infection terms and transition dynamics, respectively:

$$F = \begin{pmatrix} \frac{(\beta_1-\lambda_h)S_h}{N_h} & \frac{(\beta_2-\lambda_h)S_h}{N_h} & \frac{\beta_3 S_h}{N_h} \\ 0 & 0 & 0 \\ 0 & 0 & \frac{(\beta_4-\lambda_r)S_r}{N_r} \end{pmatrix}, \qquad V = \begin{pmatrix} m_1 & 0 & 0 \\ -\gamma_h & m_2 & 0 \\ 0 & 0 & m_3 \end{pmatrix}.$$

Evaluating matrices F and V at the DFE (11), we get

$$\mathbb{F} = \begin{pmatrix} \beta_1 & \beta_2 & \beta_3 \\ 0 & 0 & 0 \\ 0 & 0 & \beta_4 \end{pmatrix}, \qquad \mathbb{V} = \begin{pmatrix} m_1 & 0 & 0 \\ -\gamma_h & m_2 & 0 \\ 0 & 0 & m_3 \end{pmatrix}.$$

The NGM is then computed as

$$K = \mathbb{F}\mathbb{V}^{-1} = \begin{pmatrix} \frac{\beta_1 m_2 + \beta_2 \gamma_h}{m_1 m_2} & \frac{\beta_2}{m_2} & \frac{\beta_3}{m_3} \\ 0 & 0 & 0 \\ 0 & 0 & \frac{\beta_4}{m_3} \end{pmatrix}.$$

The eigenvalues of matrix K are

$$\zeta_1 = 0, \quad \zeta_2 = \frac{\beta_1 m_2 + \beta_2 \gamma_h}{m_1 m_2}, \quad \text{and } \zeta_3 = \frac{\beta_4}{m_3}.$$

Accordingly, the basic reproduction number is given by

$$\mathcal{R}_0 = \max\left\{\mathcal{R}_0^h, \mathcal{R}_0^r\right\} = \max\left\{\frac{\beta_1 m_2 + \beta_2 \gamma_h}{m_1 m_2}, \frac{\beta_4}{m_3}\right\}. \tag{13}$$

Next, we derive the endemic equilibria of model (1), which represent the long-term persistence of Mpox within the population. Model (1) admits two distinct endemic equilibrium states: The

human-endemic equilibrium (HEE) and the endemic equilibrium (EE). The HEE corresponds to a scenario in which Mpox persists solely in the human population while the rodent population remains uninfected, that is, $A_h \neq 0$, $I_h \neq 0$, but $I_r = 0$. Under these conditions, the HEE is denoted by

$$X^+ = (S_h^+, A_h^+, I_h^+, R_h^+, S_r^+, I_r^+), \tag{14}$$

with component expressions

$$S_h^+ = \frac{\pi_h}{\lambda_h^+ + \mu_h}, \quad A_h^+ = \frac{\pi_h \lambda_h^+}{(\lambda_h^+ + \mu_h)m_1}, \quad I_h^+ = \frac{\pi_h \gamma_h \lambda_h^+}{(\lambda_h^+ + \mu_h)m_1 m_2},$$
$$R_h^+ = \frac{\pi_h \gamma_h \lambda_h^+ \tau}{(\lambda_h^+ + \mu_h)m_1 m_2 \mu_h}, \quad S_r^+ = \frac{\pi_r}{\mu_r}, \quad I_r^+ = 0,$$

where the infection rate λ_h^+ is given by

$$\lambda_h^+ = \frac{m_1 m_2 \mu_h (\mathcal{R}_0^h - 1)}{m_2 \mu_h + \gamma_h \mu_h + \gamma_h \tau}.$$

It follows that the HEE exists if and only if $\mathcal{R}_0^h > 1$, indicating that the basic reproduction number for humans must exceed unity for sustained transmission in the human population.

In contrast, the EE describes a state in which both humans and rodents are endemically infected, that is, $A_h \neq 0$, $I_h \neq 0$, and $I_r \neq 0$. The EE is denoted by

$$X^* = (S_h^*, A_h^*, I_h^*, R_h^*, S_r^*, I_r^*), \tag{15}$$

with component expressions

$$S_h^* = \frac{\pi_h}{\lambda_h^* + \mu_h}, \quad A_h^* = \frac{\pi_h \lambda_h^*}{(\lambda_h^* + \mu_h)m_1}, \quad I_h^* = \frac{\pi_h \gamma_h \lambda_h^*}{(\lambda_h^* + \mu_h)m_1 m_2},$$
$$R_h^* = \frac{\pi_h \gamma_h \lambda_h^* \tau}{(\lambda_h^* + \mu_h)m_1 m_2 \mu_h}, \quad S_r^* = \frac{\pi_r}{\lambda_r^* + \mu_r}, \quad I_r^* = \frac{\pi_r \lambda_r^*}{(\lambda_r^* + \mu_r)m_3},$$

where the infection rate for rodents is given by

$$\lambda_r^* = m_3(\mathcal{R}_0^r - 1),$$

and the infection rate λ_h^* for humans is determined as the positive root of the quadratic equation

$$a{\lambda_h^*}^2 + b\lambda_h^* + c = 0,$$

where the coefficients a, b, and c are constants with respect to λ_h^* and are given by

$$a = \pi_h m_3(\lambda_r^* + \mu_r)(m_2\mu_h + \gamma_h\mu_h + \gamma_h\tau),$$
$$b = \pi_h m_1 m_2 m_3 \mu_h(\lambda_r^* + \mu_r)(1 - \mathcal{R}_0^h) - \beta_3\pi_r\lambda_r^*\mu_h m_1 m_2,$$
$$c = -\beta_3\pi_r\lambda_r^*\mu_h^2 m_1 m_2.$$

When $\mathcal{R}_0^r = 1$, the equilibrium reduces to $X^* = X^+$. Therefore, the condition $\mathcal{R}_0^r > 1$ is required to ensure that $\lambda_r^* > 0$. Given that all model parameters are strictly positive, this directly implies that $a > 0$ and $c < 0$. This guarantees the existence of a unique positive solution for λ_h^*. Therefore, the existence and uniqueness of the EE are ensured if and only if $\mathcal{R}_0^r > 1$.

3.2 Stability of disease-free equilibrium

In this section, we investigate both the local and global asymptotic stability of the DFE of model (1). The local stability analysis is carried out via linearization of the system around the DFE, using the Jacobian matrix, as stated in Theorem 2.

Theorem 2. The DFE of model (1) is locally asymptotically stable if and only if $\mathcal{R}_0 < 1$.

Proof. The Jacobian matrix associated with model (1) is expressed as

$$J = \begin{pmatrix} A - \lambda_h - \mu_h & B_1 & B_2 & A & A & C \\ -A + \lambda_h & -B_1 - m_1 & -B_2 & -A & -A & -C \\ 0 & \gamma_h & -m_2 & 0 & 0 & 0 \\ 0 & 0 & \tau & -\mu_h & 0 & 0 \\ 0 & 0 & 0 & 0 & D - \lambda_r - \mu_r & E \\ 0 & 0 & 0 & 0 & -D + \lambda_r & -E - m_3 \end{pmatrix}, \tag{16}$$

with $A = \frac{\lambda_h S_h}{N_h}, B_i = \frac{(\lambda_h - \beta_i)S_h}{N_h}, C = \frac{-\beta_3 S_h}{N_h}, D = \frac{\lambda_r S_r}{N_r}, E = \frac{(\lambda_r - \beta_4)S_r}{N_r}$, and m_1, m_2, m_3 as defined in equation (10).
Evaluating the Jacobian matrix at the DFE (11), we obtain

$$J(X^0) = \begin{pmatrix} -\mu_h & -\beta_1 & -\beta_2 & 0 & 0 & -\beta_3 \\ 0 & \beta_1 - m_1 & \beta_2 & 0 & 0 & \beta_3 \\ 0 & \gamma_h & -m_2 & 0 & 0 & 0 \\ 0 & 0 & \tau & -\mu_h & 0 & 0 \\ 0 & 0 & 0 & 0 & -\mu_r & -\beta_4 \\ 0 & 0 & 0 & 0 & 0 & \beta_4 - m_3 \end{pmatrix}.$$

The characteristic equation corresponding to matrix $J(X^0)$ is given by

$$(\mu_h + \zeta)^2(\mu_r + \zeta)(-\beta_4 + m_3 + \zeta)(\zeta^2 + k_1\zeta + k_2) = 0, \tag{17}$$

where

$$k_1 = \frac{m_2^2 + \beta_2\gamma_h + m_1m_2(1 - \mathcal{R}_0^h)}{m_2} \text{ and } k_2 = m_1m_2(1 - \mathcal{R}_0^h).$$

This yields the eigenvalues $\zeta_1 = \zeta_2 = -\mu_h, \zeta_3 = -\mu_r, \zeta_4 = m_3(\mathcal{R}_0^r - 1)$, along with the roots of the quadratic equation

$$\zeta^2 + k_1\zeta + k_2 = 0. \tag{18}$$

It is evident that $\zeta_1, \zeta_2, \zeta_3 < 0$, and that $\zeta_4 < 0$ if and only if $\mathcal{R}_0^r < 1$. Furthermore, by applying the Routh–Hurwitz criterion, the roots of (18) possess negative real parts if and only if $k_1 > 0$ and $k_2 > 0$, which holds when $\mathcal{R}_0^h < 1$. Thus, the DFE is locally asymptotically stable if and only if $\mathcal{R}_0 < 1$. □

To assess the global asymptotic stability of the DFE, we construct a Lyapunov function, as formulated in Theorem 3.

Theorem 3. The DFE of model (1) is globally asymptotically stable if and only if $\mathcal{R}_0 < 1$.

Proof. Consider the Lyapunov function $L : D \to \mathbb{R}$ defined by

$$L = c_1A_h + c_2I_h + c_3I_r, \tag{19}$$

where $c_1, c_2, c_3 > 0$.
At the DFE, it holds that $L(X^0) = 0$, while $L > 0$ for all other states in the domain. Differentiating L with respect to time yields

$$\frac{\partial L}{\partial t} \leq (c_1(\beta_1 - m_1) + c_2\gamma_h)\, A_h + (c_1\beta_2 - c_2m_2)\, I_h + (c_1\beta_3 + c_3(\beta_4 - m_3))\, I_r. \tag{20}$$

To remove the coefficient of A_h, we set

$$c_1 = \frac{m_2\gamma_h}{\beta_2\gamma_h + m_1m_2(1-\mathcal{R}_0^h)}, \quad c_2 = 1,$$

under the condition $\mathcal{R}_0^h < 1$.
Next, we choose

$$c_3 = \frac{\beta_3 m_2}{\beta_2 m_3(1-\mathcal{R}_0^r)},$$

under the condition $\mathcal{R}_0^r < 1$.
Substituting c_1, c_2, and c_3 into inequality (20) gives

$$\frac{\partial L}{\partial t} \leq -\frac{m_1m_2^2(1-\mathcal{R}_0^h)}{\beta_2\gamma_h + m_1m_2(1-\mathcal{R}_0^h)} I_h - \frac{\beta_3 m_1 m_2^2(1-\mathcal{R}_0^h)}{\beta_2^2\gamma_h + \beta_2 m_1 m_2(1-\mathcal{R}_0^h)} I_r. \tag{21}$$

Since $\mathcal{R}_0^h < 1$, it can be concluded that $\frac{\partial L}{\partial t} < 0$ for all $X \neq X^0$, and $\frac{\partial L}{\partial t} = 0$ only when the state lies at the DFE. Therefore, by LaSalle's invariance principle [21], the DFE is globally asymptotically stable if and only if $\mathcal{R}_0 < 1$. □

3.3 Global stability of endemic equilibrium

We now proceed to analyze the global asymptotic stability of the HEE of model (1), employing a Lyapunov function approach, as established in Theorem 4.

Theorem 4. Let the HEE exist, which occurs when $\mathcal{R}_0^h > 1$. The HEE of model (1) is globally asymptotically stable if and only if $\mathcal{R}_0^r < 1$.

Proof. Consider the Lyapunov function $L : D \to \mathbb{R}$ defined by

$$\begin{aligned} L = &\left(S_h - S_h^+ - S_h^+ \ln \frac{S_h}{S_h^+}\right) + \left(A_h - A_h^+ - A_h^+ \ln \frac{A_h}{A_h^+}\right) \\ &+ c_1\left(I_h - I_h^+ - I_h^+ \ln \frac{I_h}{I_h^+}\right) + c_2\left(S_r - S_r^+ - S_r^+ \ln \frac{S_r}{S_r^+}\right) + c_3 I_r, \end{aligned} \tag{22}$$

where $c_1 = \frac{\beta_2 I_h^+ S_h^+}{\gamma_h A_h^+ N_h^+}$, $c_2 = \frac{S_r^+}{\beta_4}$, and $c_3 = \frac{S_r^+}{m_3(1-\mathcal{R}_0^r)}$ under the condition $\mathcal{R}_0^r < 1$.
Denoting logarithmic expressions by L_1 through L_4, it is evident that $L(X^+) = L_1^+ + L_2^+ + c_1 L_3^+ + c_2 L_4^+ + c_3 I_r^+ = 0$, while $L > 0$ for all $X \neq X^+$, due to the convex nature of each component. This

ensures that the Lyapunov function is positive definite with respect to the HEE. Differentiating L with respect to time yields

$$\begin{aligned}\frac{\partial L}{\partial t} =& \left(1-\frac{S_h^+}{S_h}\right)\frac{dS_h}{dt} + \left(1-\frac{A_h^+}{A_h}\right)\frac{dA_h}{dt} + c_1\left(1-\frac{I_h^+}{I_h}\right)\frac{dI_h}{dt} \\ &+ c_2\left(1-\frac{S_r^+}{S_r}\right)\frac{dS_r}{dt} + c_3\frac{dI_r}{dt}. \end{aligned} \tag{23}$$

Substituting model (1) into equation (23), we get

$$\begin{aligned}\frac{\partial L}{\partial t} =& \left(1-\frac{S_h^+}{S_h}\right)\left((\lambda_h^+ + \mu_h)S_h^+ - (\lambda_h+\mu_h)S_h\right) \\ &+ \left(1-\frac{A_h^+}{A_h}\right)\left(\lambda_h S_h - \frac{\lambda_h^+ S_h^+}{A_h^+}A_h\right) + c_1\left(1-\frac{I_h^+}{I_h}\right)\left(\gamma_h A_h - \frac{\gamma_h A_h^+}{I_h^+}I_h\right) \\ &+ c_2\left(1-\frac{S_r^+}{S_r}\right)\left((\lambda_r^+ + \mu_r)S_r^+ - (\lambda_r+\mu_r)S_r\right) + c_3\left(\lambda_r S_r - m_3 I_r\right),\end{aligned}$$

which implies

$$\begin{aligned}\frac{\partial L}{\partial t} =& \mu_h S_h^+\left(2-\frac{S_h}{S_h^+}-\frac{S_h^+}{S_h}\right) + \frac{\beta_1 A_h^+ S_h^+}{N_h^+}\left(2-\frac{S_h^+}{S_h}-\frac{A_h}{A_h^+}\right) \\ &+ \frac{\beta_1 A_h^+ S_h^+}{N_h}\left(\frac{A_h}{A_h^+}-\frac{S_h}{S_h^+}\right) + \frac{\beta_2 I_h^+ S_h^+}{N_h^+}\left(2-\frac{S_h^+}{S_h}-\frac{A_h}{A_h^+}\right) \\ &+ \frac{\beta_2 I_h^+ S_h^+}{N_h}\left(\frac{I_h}{I_h^+}-\frac{S_h A_h^+ I_h}{S_h^+ A_h I_h^+}\right) + \frac{\beta_2 I_h^+ S_h^+}{N_h^+}\left(1-\frac{I_h}{I_h^+}-\frac{A_h I_h^+}{A_h^+ I_h}+\frac{A_h}{A_h^+}\right) \\ &+ \frac{\beta_3 I_r S_h^+}{N_h}\left(1-\frac{S_h A_h^+}{S_h^+ A_h}\right) + \frac{\mu_r {S_r^+}^2}{\beta_4}\left(2-\frac{S_r}{S_r^+}-\frac{S_r^+}{S_r}\right) \\ &+ \frac{I_r {S_r^+}^2}{N_r}\left(1-\frac{S_r}{S_r^+}\right) + \frac{I_r S_r^+}{m_3-\beta_4}\left(\frac{\beta_4 S_r}{N_r}-m_3\right).\end{aligned}$$

By applying algebraic simplification under the assumptions $N_h = N_h^+$, $N_r = N_r^+$, $S_r \le S_r^+$, and inequalities such as $\frac{S_h^+}{S_h} + \frac{A_h}{A_h^+} \le 2$, we obtain

$$\begin{aligned}\frac{\partial L}{\partial t} \le& \mu_h S_h^+\left(2-\frac{S_h}{S_h^+}-\frac{S_h^+}{S_h}\right) + \frac{\beta_1 A_h^+ S_h^+}{N_h^+}\left(2-\frac{S_h}{S_h^+}-\frac{S_h^+}{S_h}\right) \\ &+ \frac{\beta_2 I_h^+ S_h^+}{N_h^+}\left(3-\frac{S_h^+}{S_h}-\frac{A_h I_h^+}{A_h^+ I_h}-\frac{S_h A_h^+ I_h}{S_h^+ A_h I_h^+}\right) \\ &+ \frac{\beta_3 I_r S_h^+}{N_h^+}\left(3-\frac{S_h^+}{S_h}-\frac{A_h}{A_h^+}-\frac{S_h A_h^+}{S_h^+ A_h}\right)\end{aligned}$$

$$+\frac{\mu_r {S_r^+}^2}{\beta_4}\left(2-\frac{S_r}{S_r^+}-\frac{S_r^+}{S_r}\right)-I_rS_r. \tag{24}$$

By utilizing the arithmetic-geometric mean inequality, we get

$$\left(2-\frac{S_h}{S_h^+}-\frac{S_h^+}{S_h}\right)\le 0, \qquad \left(3-\frac{S_h^+}{S_h}-\frac{A_hI_h^+}{A_h^+I_h}-\frac{S_hA_h^+I_h}{S_h^+A_hI_h^+}\right)\le 0,$$
$$\left(3-\frac{S_h^+}{S_h}-\frac{A_h}{A_h^+}-\frac{S_hA_h^+}{S_h^+A_h}\right)\le 0, \qquad \left(2-\frac{S_r}{S_r^+}-\frac{S_r^+}{S_r}\right)\le 0.$$

Therefore, $\frac{\partial L}{\partial t}<0$ if and only if $\mathcal{R}_0^r<1$, and $\frac{\partial L}{\partial t}=0$ only at the HEE. By applying LaSalle's invariance principle [21], we conclude that the HEE is globally asymptotically stable if and only if $\mathcal{R}_0^r<1$. □

Next, we analyze the global asymptotic stability of the EE, as stated in Theorem 5.

Theorem 5. Let the EE exist, which occurs when $\mathcal{R}_0^r>1$. The EE of model (1) is globally asymptotically stable.

Proof. Consider the Lyapunov function $L\colon D\to\mathbb{R}$ defined by

$$\begin{aligned}L=&\left(S_h-S_h^*-S_h^*\ln\frac{S_h}{S_h^*}\right)+\left(A_h-A_h^*-A_h^*\ln\frac{A_h}{A_h^*}\right)\\&+c\left(I_h-I_h^*-I_h^*\ln\frac{I_h}{I_h^*}\right)\\&+\left(S_r-S_r^*-S_r^*\ln\frac{S_r}{S_r^*}\right)+\left(I_r-I_r^*-I_r^*\ln\frac{I_r}{I_r^*}\right),\end{aligned} \tag{25}$$

where $c=\frac{\beta_2 I_h^*S_h^*}{\gamma_h A_h^*N_h^*}$.
Clearly, $L(X^*)=L_1^*+L_2^*+cL_3^*+L_4^*+L_5^*=0$, and $L>0$ for all $X\neq X^*$, as each component is positive definite. Differentiating L with respect to time yields

$$\begin{aligned}\frac{\partial L}{\partial t}=&\left(1-\frac{S_h^*}{S_h}\right)\frac{dS_h}{dt}+\left(1-\frac{A_h^*}{A_h}\right)\frac{dA_h}{dt}+c\left(1-\frac{I_h^*}{I_h}\right)\frac{dI_h}{dt}\\&+\left(1-\frac{S_r^*}{S_r}\right)\frac{dS_r}{dt}+\left(1-\frac{I_r^*}{I_r}\right)\frac{dI_r}{dt}.\end{aligned} \tag{26}$$

By using the same reasoning adopted in the proof of Theorem 4, then assuming $N_h=N_h^*$, $N_r=N_r^*$, and inequality $\frac{I_r}{I_r^*}+\frac{I_r^*}{I_r}\le 2$, we obtain

$$\frac{\partial L}{\partial t}\le \mu_hS_h^*\left(2-\frac{S_h}{S_h^*}-\frac{S_h^*}{S_h}\right)+\frac{\beta_1A_h^*S_h^*}{N_h^*}\left(2-\frac{S_h}{S_h^*}-\frac{S_h^*}{S_h}\right)$$

$$+\frac{\beta_2 I_h^* S_h^*}{N_h^*}\left(3-\frac{S_h^*}{S_h}-\frac{A_h I_h^*}{A_h^* I_h}-\frac{S_h A_h^* I_h}{S_h^* A_h I_h^*}\right)$$
$$+\frac{\beta_3 I_r^* S_h^*}{N_h^*}\left(4-\frac{S_h^*}{S_h}-\frac{A_h}{A_h^*}-\frac{I_r^*}{I_r}-\frac{S_h A_h^* I_r}{S_h^* A_h I_r^*}\right)$$
$$+\frac{\beta_4 I_r^* S_r^*}{N_r^*}\left(2-\frac{S_r}{S_r^*}-\frac{S_r^*}{S_r}\right)+\mu_r S_r^*\left(2-\frac{S_r}{S_r^*}-\frac{S_r^*}{S_r}\right). \tag{27}$$

By utilizing the arithmetic-geometric mean inequality, we get

$$\left(2-\frac{S_h}{S_h^*}-\frac{S_h^*}{S_h}\right)\le 0, \qquad \left(3-\frac{S_h^*}{S_h}-\frac{A_h I_h^*}{A_h^* I_h}-\frac{S_h A_h^* I_h}{S_h^* A_h I_h^*}\right)\le 0,$$
$$\left(4-\frac{S_h^*}{S_h}-\frac{A_h}{A_h^*}-\frac{I_r^*}{I_r}-\frac{S_h A_h^* I_r}{S_h^* A_h I_r^*}\right)\le 0, \qquad \left(2-\frac{S_r}{S_r^*}-\frac{S_r^*}{S_r}\right)\le 0.$$

Therefore, $\frac{\partial L}{\partial t}<0$ for all $X\neq X^*$, and $\frac{\partial L}{\partial t}=0$ only at the EE. By LaSalle's invariance principle [21], we conclude that the EE is globally asymptotically stable. □

4 Application of the model to real data

4.1 Parameter estimation

In this study, we utilized cumulative case data of Mpox infections in the United States (U.S.), spanning from June 1, 2022, to September 30, 2022, obtained from the official Centers for Disease Controls and Prevention (CDC) website [13]. According to the National Vital Statistics System, life expectancy in the United States in 2022 was 77.5 years, while the U.S. Census Bureau reported the total population as 333,287,557 individuals. Consequently, parameters π_h and μ_h are derived as follows:

$$\mu_h=\frac{1}{\text{life expectancy}}=\frac{1}{77.5\times 365}=\frac{1}{28287.5}=3.535\times 10^{-5}\ /\text{day},$$

$$\pi_h=\mu_h\times\text{total population}=\frac{333287557}{28287.5}=11782.149\ \text{individuals/day}.$$

The remaining parameters are estimated using the nonlinear least squares method. This procedure aimed to determine the optimal parameters by minimizing the sum of squared deviations between the observed data and the model predictions. The initial conditions are set as follows: $S_h(0)=333287548,\ A_h(0)=0,\ I_h(0)=9,\ R_h(0)=0,\ S_r(0)=800,\ I_r(0)=10.$

Figure 2 compares the cumulative number of Mpox infections from the reported data and the values from the fitted model. The model fits the empirical data well during most of the observation period. This agreement shows that the applied parameter set and the estimation strategy have captured the essence of the transmission dynamics of Mpox. Furthermore, the close proximity of the simulated curve to the reported data points reflects the robustness of the model in mimicking the epidemic curve of cumulative incidence, hence validating the suitability of the model for further forecasting and policy-oriented analyses.

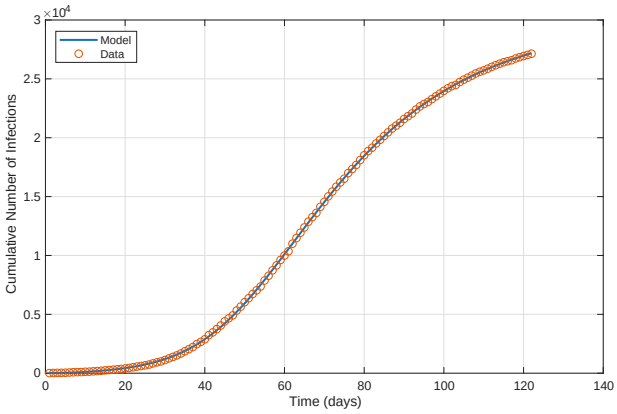

Figure 2: Comparison of model simulation and reported data for cumulative Mpox infections over time

The obtained mean absolute percentage error is 3.645%, indicating that the parameter estimation results exhibit a high level of accuracy and reliability. Referring to the estimated parameters presented in Table 3, the basic reproduction numbers are calculated as $\mathcal{R}_0^h = 0.88235$ for the human population and $\mathcal{R}_0^r = 2.08405$ for the rodent population, resulting in an overall basic reproduction number of $\mathcal{R}_0 = 2.08405$. Since the value of $\mathcal{R}_0$ exceeds unity, the model suggests that Mpox continues to persist in an endemic state within the United States.

Table 3: Parameter values

Parameter	Value	Parameter	Value
π_r	150.78	τ	0.11385
β_1	0.37198	δ_1	0.08249
β_2	0.07489	δ_2	0.07999
β_3	0.93455	δ_3	0.00011
β_4	0.19412	μ_r	0.09304
γ_h	0.60306		

4.2 Sensitivity analysis

In this section, a sensitivity analysis is carried out to determine the parameters that exert the greatest influence on the stability conditions of the equilibrium points in model (1). The sensitivity index corresponding to each parameter is evaluated using the relation $e_x = \frac{x}{\mathcal{R}_0} \times \frac{\partial \mathcal{R}_0}{\partial x}$, where x, $\mathcal{R}_0$, and e_x represent the parameter under consideration, the basic reproduction number, and the sensitivity index of x with respect to $\mathcal{R}_0$, respectively. A positive sensitivity index indicates that an increase (decrease) in the parameter value will lead to an increase (decrease) in $\mathcal{R}_0$. In contrast, a negative sensitivity index suggests that an increase (decrease) in the parameter value results in a decrease (increase) in $\mathcal{R}_0$. According to the parameter values in Table 3, the computed sensitivity indices for the parameters contributing to $\mathcal{R}_0$ are presented in Table 4.

Table 4: Sensitivity indices

Parameter	Sensitivity index on $\mathcal{R}_0^h$	Sensitivity index on $\mathcal{R}_0^r$
β_1	0.61491	–
β_2	0.38509	–
β_4	–	1
γ_h	−0.49454	–
τ	−0.22613	–
δ_1	−0.12032	–
δ_2	−0.15888	–
δ_3	–	−0.00118
μ_h	−0.00012	–
μ_r	–	−0.99882

As presented in Table 4, parameters β_1 and β_2 demonstrate positive sensitivity indices with respect to $\mathcal{R}_0^h$, implying that an increase in these parameters leads to a higher value of $\mathcal{R}_0^h$. Conversely, parameters γ_h, τ, δ_1, δ_2, and μ_h exhibit negative sensitivity indices, indicating that their increase reduces the value of $\mathcal{R}_0^h$. With regard to $\mathcal{R}_0^r$, only β_4 shows a positive sensitivity index, while δ_3 and μ_r display negative values. In general, β_1 and γ_h emerge as the most influential parameters on $\mathcal{R}_0^h$, as they possess the largest absolute sensitivity indices. The influence of parameters β_1 and γ_h is illustrated in Figure 3. For $\mathcal{R}_0^r$, the parameters with the greatest impact are β_4 and μ_r. Nevertheless, since the natural mortality rate of rodents (μ_r) is typically beyond human control, the most relevant intervention strategies should focus on β_4 and δ_3 within the rodent population.

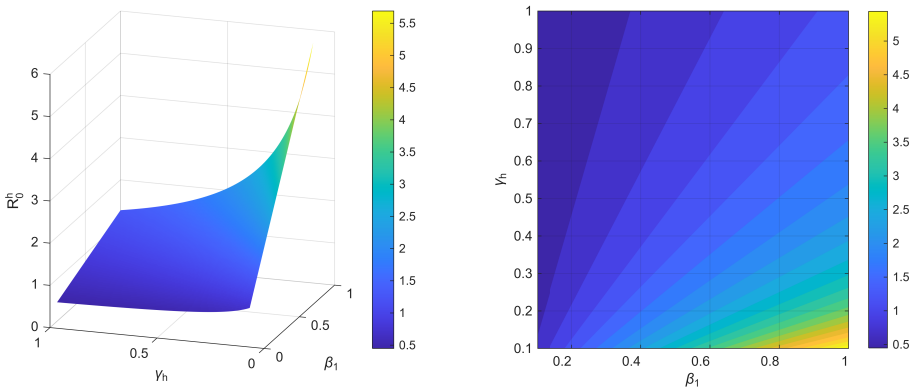

Figure 3: Influence of parameters β_1 and γ_h with respect to $\mathcal{R}_0^h$

4.3 Numerical simulation

In this section, numerical simulations are conducted to investigate the influence of parameters β_1 and γ_h on the dynamics of both A_h and I_h within the time horizon from $t = 0$ to $t = 500$ days. The outcomes of these simulations are illustrated in Figures 4 and 5. Figure 4 illustrates the temporal dynamics of the asymptomatic (A_h) and symptomatic (I_h) human subpopulations under varying values of the transmission parameter β_1. As observed, higher values of β_1 substantially accelerate the epidemic growth rate and lead to significantly larger equilibrium levels in both compartments. Specifically, when $\beta_1 = 0.4$, the prevalence of A_h and I_h reaches markedly higher peaks compared to scenarios with $\beta_1 = 0.3$ and $\beta_1 = 0.35$, followed by a gradual decline over time. On the other hand, smaller values of β_1 weaken the speed of an epidemic and stabilize with lower intensities, indicating that transmission intensity significantly controls the magnitude and persistence of infection in humans. These observations highlight that β_1 plays a paramount role in shaping disease burden and long-term epidemic outcomes.

The short-term dynamics (right panels) of Figure 5 illustrate the early behavior of the asymptomatic (A_h) and symptomatic (I_h) human subpopulations under varying values of the transition rate γ_h, which represents the progression rate of Mpox from the asymptomatic to symptomatic phase. For A_h, lower γ_h values (e.g., 0.1 and 0.3) lead to a slower depletion of the asymptomatic compartment, allowing a higher accumulation of infectious individuals and a sustained transmission potential. In contrast, higher γ_h (e.g., 1) rapidly converts A_h into I_h, leading to an initially faster rise in symptomatic cases. However, for I_h, this trend reverses over time: Although high γ_h causes an early peak in symptomatic individuals, the rapid depletion of A_h reduces the continued inflow into I_h, resulting in an eventual decline or stabilization. Meanwhile, lower γ_h values

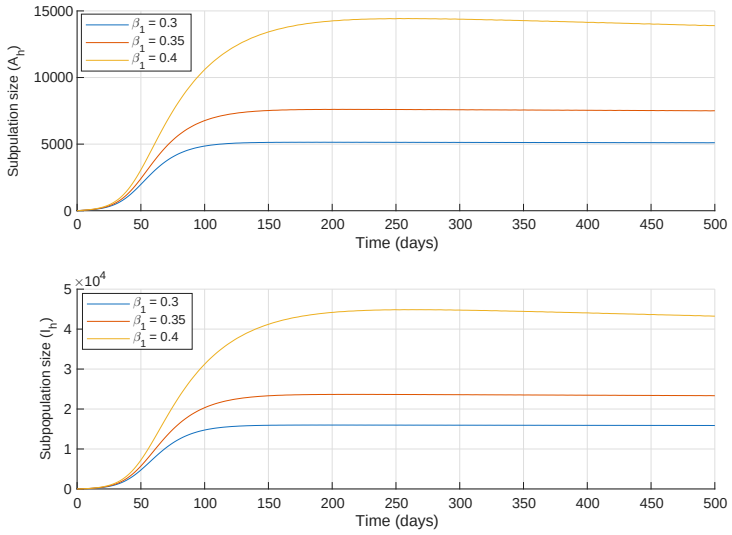

Figure 4: Influence of parameter β_1 with respect to A_h and I_h

prolong the infectious duration of asymptomatic carriers, thereby sustaining transmission and gradually increasing the I_h population to surpass the high γ_h scenarios. The long-term dynamics (left panels) confirm this reversal: Lower γ_h values sustain elevated equilibrium levels of both A_h and I_h, while higher γ_h values result in early saturation and lower prevalence. These results emphasize a nonlinear trade-off in γ_h: Higher values accelerate clinical progression but suppress long-term transmission, while lower values prolong asymptomatic infectious periods, yielding a higher cumulative disease burden.

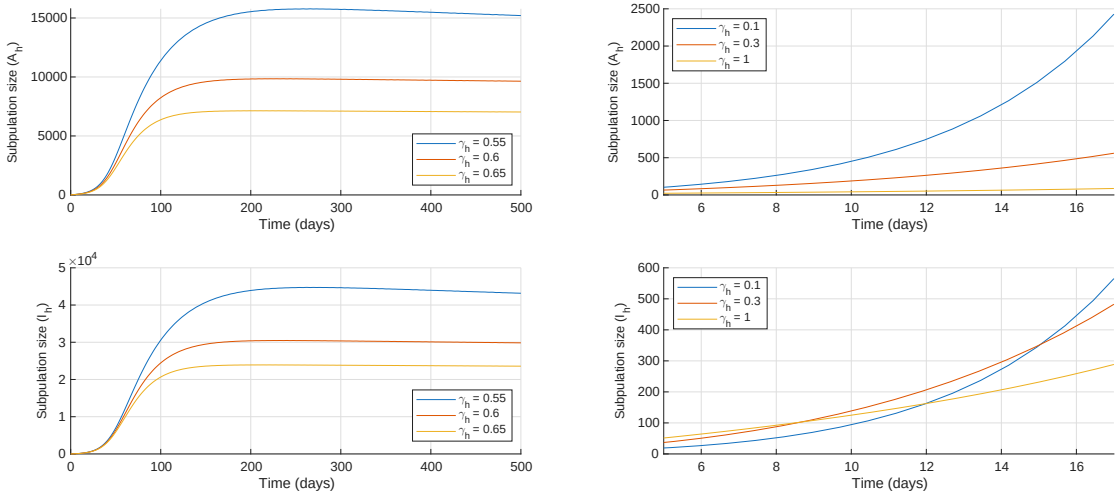

Figure 5: Influence of parameter γ_h with respect to A_h and I_h

Figure 6 depicts the temporal dynamics of the different human (S_h, A_h, I_h, R_h) and rodent (S_r, I_r) compartments from the simulated Mpox transmission model. Among the human subpopulations, the susceptible class S_h exhibits a gradual decrease in the temporal domain, whereas the recovered class R_h displays a steady increase, indicating the build-up of immunity over time. The asymptomatic (A_h) and symptomatic (I_h) compartments experience an initial increase, where I_h rises faster and remains consistently at higher levels than A_h, indicating that the majority of the human infectious pool comprises symptomatic infections. Meanwhile, the rodent dynamics exhibit a typical transient profile. The susceptible rodent pool S_r first increases, presumably due to births mediated by natural processes, then quickly decreases as infection occurs among the rodent population, and finally settles into a steady-state solution, indicating an endemic state. The infected rodent pool I_r increases during the initial phase of the outbreak, reflecting a rapid infection growth rate, then tapers off, further indicating that infection is persisting within the rodent reservoir. This suggests that interspecies interactions drive the spread of Mpox and points out the necessity of monitoring both host populations for long-term epidemic control.

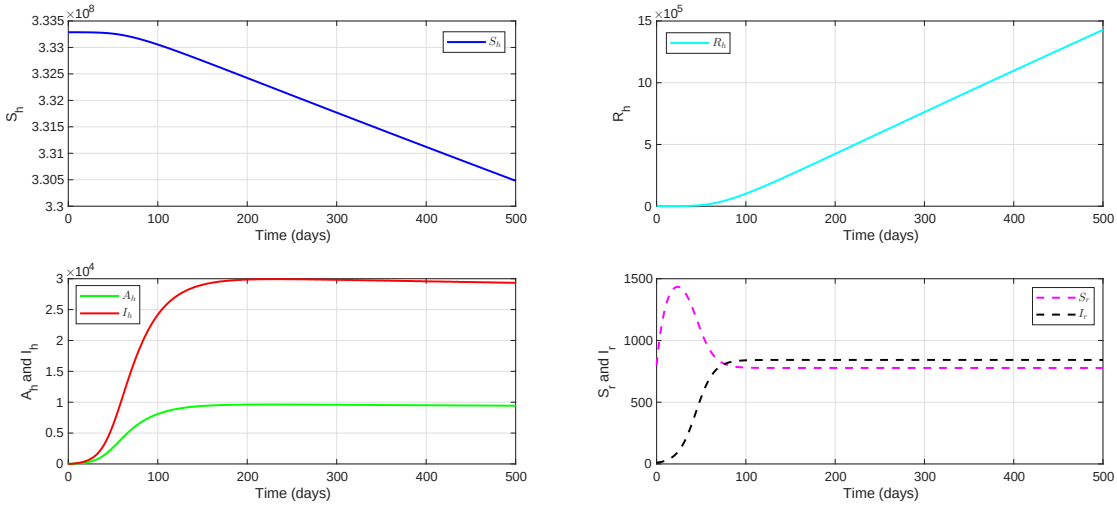

Figure 6: Dynamics of human and rodent populations

5 Optimal control

5.1 Model and characterization

This section investigates the incorporation of control measures into model (1) and subsequently analyzes the characterization of the corresponding optimal control problem. Two control measures are considered, namely vaccination and rodenticide usage. The vaccination control is represented by the time-dependent control variable $u_1(t)$, which describes vaccine administration to susceptible individuals at rate κ_1. Vaccines such as JYNNEOS are capable of inducing immunity after a certain period, thereby reducing the likelihood of infection among susceptible individuals [5]. The rodenticide usage control is represented by the time-dependent control variable $u_2(t)$, which corresponds to the targeted removal of Mpox-infected rodents at rate κ_2. This control has been recommended as a preventive strategy to limit Mpox transmission, as reported by the Leicester Mercury newspaper [23]. By incorporating these two controls, model (1) is reformulated as follows:

$$\begin{aligned}
\frac{dS_h}{dt} &= \pi_h - (\lambda_h + \mu_h + \kappa_1 u_1(t))S_h,\\
\frac{dA_h}{dt} &= \lambda_h S_h - (\gamma_h + \delta_1 + \mu_h)A_h,\\
\frac{dI_h}{dt} &= \gamma_h A_h - (\tau + \delta_2 + \mu_h)I_h,\\
\frac{dR_h}{dt} &= \kappa_1 u_1(t) S_h + \tau I_h - \mu_h R_h,\\
\frac{dS_r}{dt} &= \pi_r - (\lambda_r + \mu_r)S_r,\\
\frac{dI_r}{dt} &= \lambda_r S_r - (\delta_3 + \mu_r + \kappa_2 u_2(t))I_r,
\end{aligned} \tag{28}$$

where

$$\lambda_h = \frac{\beta_1 A_h + \beta_2 I_h + \beta_3 I_r}{N_h}, \qquad \lambda_r = \frac{\beta_4 I_r}{N_r}.$$

The optimal control problem associated with model (28) is formulated to reduce the number of asymptomatic humans (A_h), symptomatic humans (I_h), and infected rodents (I_r), while simultaneously minimizing the implementation costs of the applied controls. The vaccination control $u_1(t)$ generates costs related to vaccine procurement, distribution, and healthcare personnel. The rodenticide usage control $u_2(t)$ incurs operational costs related to labor, equipment, and chemical procurement expenses. Accordingly, the objective functional is defined by

$$F(\mathbf{x}(t), \mathbf{u}(t)) = \int_0^{t_f} \left(v_1 A_h + v_2 I_h + v_3 I_r + \frac{1}{2} \left(w_1 u_1^2(t) + w_2 u_2^2(t) \right) \right) dt, \tag{29}$$

where v_1, v_2, v_3 denote the weighting coefficients associated with the infected compartments, whereas w_1, w_2 denote the cost coefficients corresponding to the implemented control measures. The quadratic expressions $u_1^2(t)$ and $u_2^2(t)$ are introduced to preserve the convexity of the objective functional, thereby facilitating analytical treatment and ensuring the existence of an optimal solution. In addition, this formulation captures the realistic assumption that higher control intensities produce disproportionately greater implementation costs. Such a quadratic structure is also commonly employed in optimal control theory because it simplifies the derivation of optimality conditions through Pontryagin's principle. The objective is therefore to identify the optimal controls $u_1^*(t)$ and $u_2^*(t)$ that minimize the objective functional, namely,

$$F(\mathbf{x}(t), \mathbf{u}^*(t)) = \min \left\{ F(\mathbf{x}(t), \mathbf{u}(t)) \mid (u_1(t), u_2(t)) \in U \right\},$$

where the admissible control set is defined as

$$U = \left\{ (u_1(t), u_2(t)) \mid 0 \leq u_1(t) \leq 1,\ 0 \leq u_2(t) \leq 1 \right\}.$$

The optimal control problem corresponding to model (28) is established using Pontryagin's principle [14]. By employing this principle, the objective functional in (29) is transformed into the Hamiltonian function $\mathcal{H}$, which is defined as follows:

$$\begin{aligned} \mathcal{H}(\mathbf{x}(t), \mathbf{u}(t), \mathbf{p}(t), t) =& v_1 A_h + v_2 I_h + v_3 I_r + \frac{1}{2} \left(w_1 u_1^2(t) + w_2 u_2^2(t) \right) \\ &+ p_1(t)(\pi_h - (\lambda_h + \mu_h + \kappa_1 u_1(t)) S_h) \\ &+ p_2(t)(\lambda_h S_h - (\gamma_h + \delta_1 + \mu_h) A_h) \\ &+ p_3(t)(\gamma_h A_h - (\tau + \delta_2 + \mu_h) I_h) \\ &+ p_4(t)(\kappa_1 u_1(t) S_h + \tau I_h - \mu_h R_h) \\ &+ p_5(t)(\pi_r - (\lambda_r + \mu_r) S_r) \\ &+ p_6(t)(\lambda_r S_r - (\delta_3 + \mu_r + \kappa_2 u_2(t)) I_r), \end{aligned} \tag{30}$$

where $p_i(t)$ for $i = 1, 2, \ldots, 6$ denote the costate variables.

Based on Pontryagin's principle, an optimal solution satisfies the conditions given by the state equations, costate equations, and stationary conditions of the Hamiltonian function. The state equations in model (28) are obtained from the partial derivatives of $\mathcal{H}$ with respect to the costate variables. Meanwhile, the costate equations are obtained from the negative partial derivatives of

$\mathcal{H}$ with respect to the state variables and are formulated as

$$\begin{aligned}
\frac{dp_1(t)}{dt} &= (p_1(t)-p_2(t))\left(\lambda_h - \frac{\lambda_h S_h}{N_h}\right) + p_1(t)(\mu_h + \kappa_1 u_1(t)) - p_4(t)\kappa_1 u_1(t),\\
\frac{dp_2(t)}{dt} &= -v_1 + (p_1(t)-p_2(t))\left(\frac{\beta_1 - \lambda_h}{N_h}\right) S_h + p_2(t)(\gamma_h + \delta_1 + \mu_h)\\
&\quad - p_3(t)\gamma_h,\\
\frac{dp_3(t)}{dt} &= -v_2 + (p_1(t)-p_2(t))\left(\frac{\beta_2 - \lambda_h}{N_h}\right) S_h + p_3(t)(\tau + \delta_2 + \mu_h) - p_4(t)\tau,\\
\frac{dp_4(t)}{dt} &= (p_2(t)-p_1(t))\frac{\lambda_h S_h}{N_h} + p_4(t)\mu_h,\\
\frac{dp_5(t)}{dt} &= (p_5(t)-p_6(t))\left(\lambda_r - \frac{\lambda_r S_r}{N_r}\right) + p_5(t)\mu_r,\\
\frac{dp_6(t)}{dt} &= -v_3 + (p_1(t)-p_2(t))\frac{\beta_3 S_h}{N_h} + (p_5(t)-p_6(t))\left(\frac{\beta_4 - \lambda_r}{N_r}\right) S_r\\
&\quad + p_6(t)(\delta_3 + \mu_r + \kappa_2 u_2(t)),
\end{aligned} \tag{31}$$

subject to the transversality conditions $p_i(t_f) = 0$ for $i = 1, 2, \ldots, 6$. These conditions follow from Pontryagin's principle because t_f is fixed, $\mathbf{x}(t_f)$ is free, and the objective functional contains no terminal payoff term. Consequently, the costate variables p_i become zero at t_f, indicating that the marginal contribution of each state variable to the objective functional becomes zero at the end of the control period.

In addition, the stationary conditions are obtained by differentiating $\mathcal{H}$ with respect to the control variables. Therefore, the control functions $u_1(t)$ and $u_2(t)$ are represented by

$$u_1(t) = \frac{(p_1(t)-p_4(t))\kappa_1 S_h}{w_1}, \qquad u_2(t) = \frac{p_6(t)\kappa_2 I_r}{w_2}.$$

To maintain biological admissibility, each control variable is constrained within the interval $[0, 1]$. Therefore, the optimal control profiles $u_1^*(t)$ and $u_2^*(t)$ are determined as

$$\begin{aligned}
u_1^*(t) &= \min\left\{1, \max\left\{0, \frac{(p_1(t)-p_4(t))\kappa_1 S_h}{w_1}\right\}\right\},\\
u_2^*(t) &= \min\left\{1, \max\left\{0, \frac{p_6(t)\kappa_2 I_r}{w_2}\right\}\right\}.
\end{aligned} \tag{32}$$

5.2 Simulation with control

The optimal control problem associated with model (28) is solved numerically by employing the forward-backward sweep method. The parameter values presented in Table 3 are adopted in the simulations within the time horizon from $t = 0$ to $t = 500$ days. To investigate the impact of different intervention policies, three control strategies are considered in the numerical simulations. These strategies are formulated based on two control variables, namely vaccination ($u_1(t)$) and rodenticide usage ($u_2(t)$). Strategy A considers the implementation of vaccination only ($u_1(t)$), Strategy B applies rodenticide usage only ($u_2(t)$), whereas Strategy C combines vaccination and rodenticide usage simultaneously ($u_1(t), u_2(t)$). Each control strategy is evaluated by comparing it with the uncontrolled scenario to examine its effectiveness in reducing the asymptomatic human, symptomatic human, and infected rodent subpopulations.

Figure 7 illustrates the dynamics of the asymptomatic human subpopulation (A_h) under all control strategies compared with the uncontrolled scenario. It can be observed that, in the absence of control strategies, the value of A_h increases sharply from the beginning of the simulation period until approximately day 100, after which the growth rate gradually slows and eventually stabilizes until the end of the simulation period. This behavior indicates a rapid increase in A_h, thereby elevating the risk of Mpox transmission. In contrast, the implementation of control strategies significantly reduces the number of A_h, demonstrating the effectiveness of control strategies in suppressing the growth of the asymptomatic human subpopulation. Among the considered strategies, Strategy C, which combines both control strategies, appears to be the most effective, although its difference from Strategy A is relatively small.

A similar pattern is observed in the dynamics of the symptomatic human subpopulation (I_h), as illustrated in Figure 8. The value of I_h also increases rapidly in the uncontrolled scenario, while Strategy C remains the most effective approach for suppressing the growth of I_h. Furthermore, Figure 9, which presents the dynamics of the infected rodent subpopulation (I_r), exhibits behavior distinct from that of A_h and I_h. The application of Strategy A has no effect on the dynamics of I_r, as its trajectory coincides with the uncontrolled scenario. This occurs because vaccination is administered only to the susceptible human subpopulation, and there is no transmission pathway from humans to rodents. Meanwhile, Strategies B and C are highly effective in reducing the growth of I_r.

The control profiles for all strategies are presented in Figure 10. Under Strategy A, the control variable $u_1(t)$ remains at its upper bound throughout the entire simulation period. In contrast, under Strategy B, the control variable $u_2(t)$ decreases sharply starting around day 25 and reaches zero from approximately day 35 until the end of the simulation period. Under

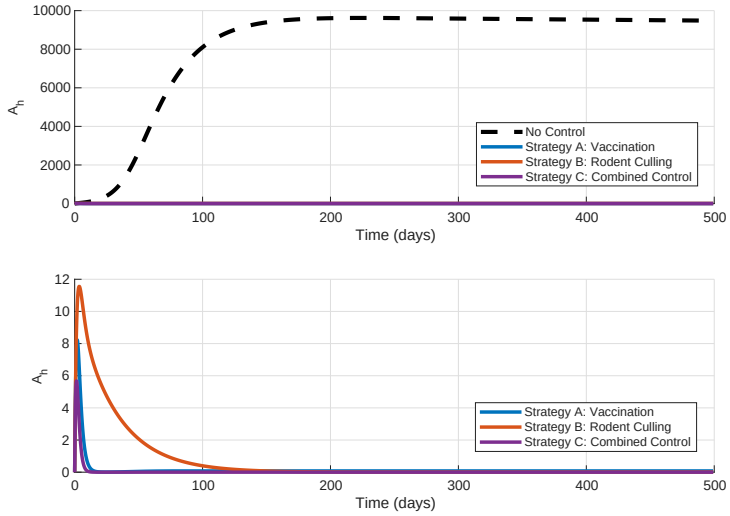

Figure 7: Dynamics of A_h under all control strategies

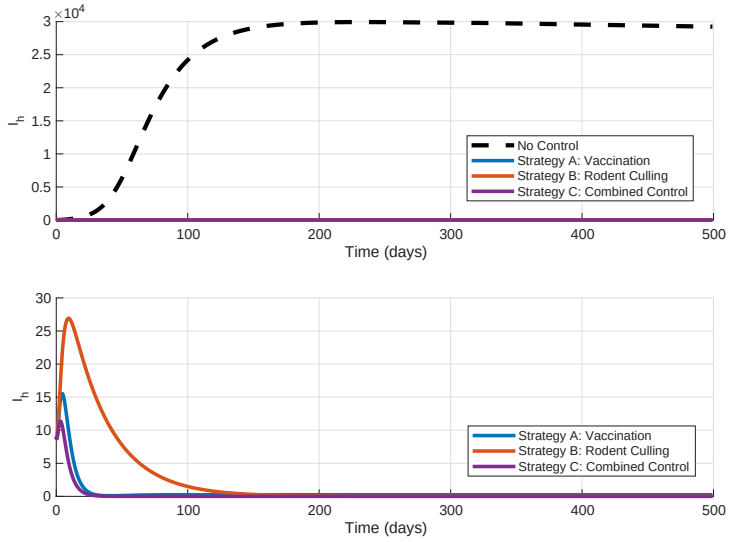

Figure 8: Dynamics of I_h under all control strategies

Strategy C, the control variable $u_1(t)$ decreases sharply first, followed by $u_2(t)$, and both controls reach zero before day 50 and remain at zero until the end of the simulation period.

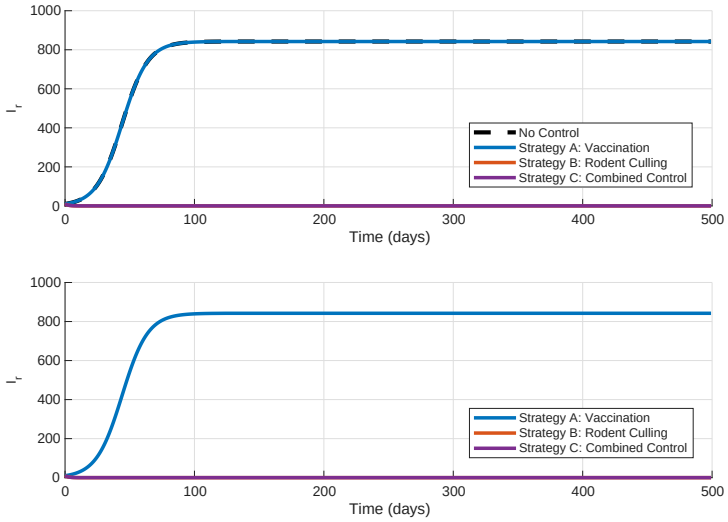

Figure 9: Dynamics of I_r under all control strategies

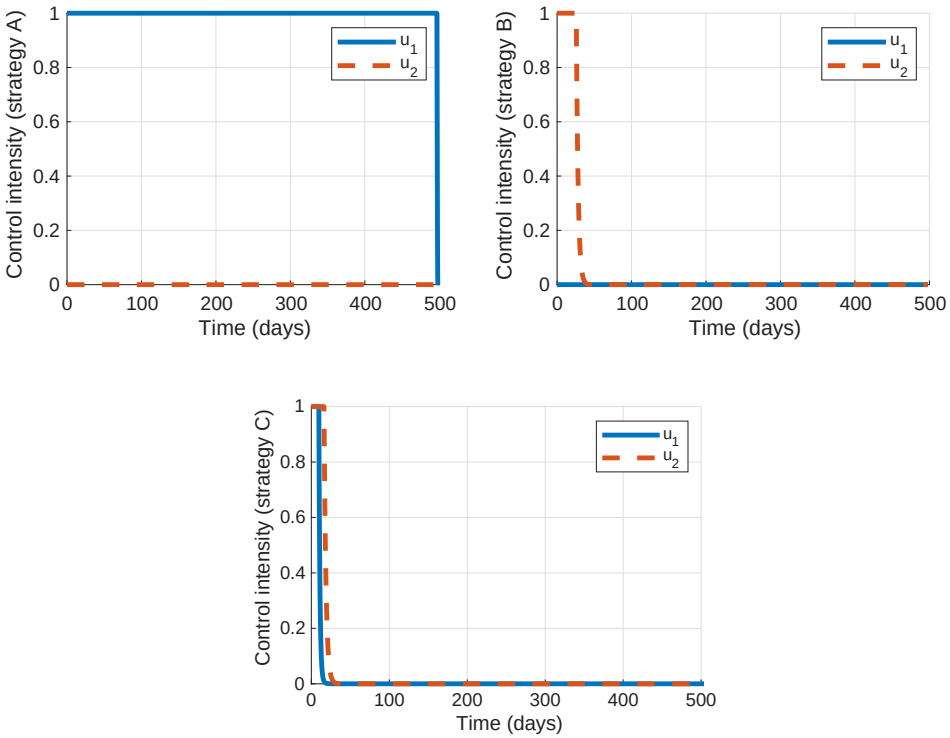

Figure 10: Control profiles for all strategies

5.3 Cost-effectiveness

Cost-effectiveness analysis evaluates the economic efficiency of control strategies by comparing their implementation costs with the corresponding health outcomes. In this section, we employ the incremental cost-effectiveness ratio (ICER) to identify the strategy that provides the greatest health benefit relative to its cost. Following [19], the ICER is defined as

$$\text{ICER} = \frac{\text{Difference in total cost between strategies } i \text{ and } j}{\text{Difference in total infections averted between strategies } i \text{ and } j}.$$

The total infections averted are estimated by subtracting the total infections occurring after the implementation of a specific control strategy from the projected total infections in the absence of any strategy. The values of the total cost and total infections averted for all strategies are presented in Table 5.

Table 5: Total cost and total infections averted

Strategy	Total cost	Total infections averted
A	13,657	1,222,500
B	24,701	1,268,800
C	12,494	1,269,500

The control strategies are first ranked according to the total number of infections averted in ascending order, starting from the strategy with the lowest number of infections averted. Subsequently, the ICER values can be calculated sequentially in the following manner:

$$\begin{aligned}
\text{ICER (A)} &= \frac{13{,}657 - 0}{1{,}222{,}500 - 0} = 0.0112,\\
\text{ICER (B)} &= \frac{24{,}701 - 13{,}657}{1{,}268{,}800 - 1{,}222{,}500} = 0.2385,\\
\text{ICER (C)} &= \frac{12{,}494 - 24{,}701}{1{,}269{,}500 - 1{,}268{,}800} = -17.4386.
\end{aligned}$$

The initial ICER calculation is performed using the ranked strategies, where Strategy B is identified as having the highest ICER value. Therefore, Strategy B is excluded from the subsequent analysis, and the ICER values are recalculated using the same approach for the remaining strategies, which are then ordered as Strategies A and C. The next ICER calculation is presented as follows:

$$\text{ICER (A)} = \frac{13{,}657 - 0}{1{,}222{,}500 - 0} = 0.0112,$$
$$\text{ICER (C)} = \frac{12{,}494 - 13{,}657}{1{,}269{,}500 - 1{,}222{,}500} = -0.0247.$$

Based on this result, Strategy C has a lower ICER value than Strategy A, suggesting that Strategy C is the most cost-effective strategy.

6 Conclusion

The SAIR-SI model of Mpox transmission developed in this study comprises six compartments: Susceptible humans (S_h), asymptomatic humans (A_h), symptomatic infected humans (I_h), recovered humans (R_h), susceptible rodents (S_r), and infected rodents (I_r). The model satisfies the well-posedness, boundedness, and nonnegativity properties. Three equilibrium points are identified: The DFE, the HEE, and the EE. The DFE is both locally and globally asymptotically stable when the basic reproduction number $\mathcal{R}_0$ is less than one. The HEE is globally asymptotically stable provided that $\mathcal{R}_0^r$ is less than one. If the EE exists, then it is globally asymptotically stable. Sensitivity analysis reveals that parameters β_1 and γ_h exert the greatest influence on $\mathcal{R}_0^h$, with β_1 positively correlated and γ_h negatively correlated with $\mathcal{R}_0^h$. Conversely, parameters β_4 and δ_3 most significantly affect $\mathcal{R}_0^r$, where β_4 shows a positive correlation and δ_3 shows a negative correlation. The results of this study reveal that key transmission parameters drive the dynamics within both human and rodent populations during outbreaks. In detail, transmission parameter β_1 significantly influences the growth rate of epidemics and equilibrium levels; higher values accelerate epidemic progression, leading to larger peaks in asymptomatic and symptomatic subpopulations, A_h and I_h, respectively. Progression rate γ_h is equally crucial, as lower values prolong asymptomatic infectious periods, thus sustaining transmission and yielding a higher cumulative disease burden, while higher values expedite clinical progression but suppress long-term transmission. Furthermore, two control measures, namely vaccination and rodenticide usage, are introduced into the model. The characterization of the optimal control is analyzed using Pontryagin's principle. Three control strategies are considered in the numerical simulations: Strategy A involves vaccination only, Strategy B applies rodenticide usage only, and Strategy C combines both control measures simultaneously. The simulation results indicate that Strategy C is the most effective approach for reducing the asymptomatic human, symptomatic human, and infected rodent subpopulations. The cost-effectiveness analysis confirms that Strategy C is also the most efficient strategy, providing valuable guidance for policymakers

in selecting a control strategy that achieves improved health outcomes while considering limited available resources.

Further research will focus on addressing the limitations of the current model by incorporating additional epidemiological factors, including age structure, sexual transmission stratification, seasonal variations, and heterogeneous mixing patterns. Moreover, the inclusion of supportive treatment control and environmental influences may further improve the model framework and enhance its predictive capability for Mpox transmission dynamics.

Acknowledgments

The authors would like to express their sincere gratitude to all those who contributed to the success of this study, including the valuable feedback from the reviewers and the editorial support provided by the journal team.

Funding

This research received no external funding.

Conflicts of Interest

The authors declare no conflicts of interest.

References

[1] Abidemi, A., Fatmawati and Peter, O.J. *An optimal control model for dengue dynamics with asymptomatic, isolation, and vigilant compartments*, Decis. Anal. J. 10 (2024), 100413.

[2] Alakunle, E., Moens, U., Nchinda, G. and Okeke, M.I. *Monkeypox virus in Nigeria: infection biology, epidemiology, and evolution*, Viruses 12 (2020), 1257.

[3] Alkhazzan, A., Wang, J., Nie, Y., Shah, S.M.A., Almutairi, D.K., Khan, H. and Alzabut, J. *Lyapunov-based analysis and worm extinction in wireless networks using stochastic SVEIR model*, Alex. Eng. J. 118 (2025), 337–353.

[4] Allehiany, F.M., Darassi, M.H., Ahmad, I., Khan, M.A. and Tag-eldin, E.M. *Mathematical modeling and backward bifurcation in monkeypox disease under real observed data*, Results Phys. 50 (2023), 106557.

[5] Alshahrani, A.M. *Cost-benefit analysis of interventions to mitigate the monkeypox virus*, Int. J. Environ. Res. Public Health 19 (2022), 13789.

[6] Alshehri, A.M. and Ullah, S. *Optimal control analysis of monkeypox disease with the impact of environmental transmission*, AIMS Math. 8 (2023), 16926–16960.

[7] Al-Shomrani, M.M., Musa, S.S. and Yusuf, A. *Unfolding the transmission dynamics of monkeypox virus: an epidemiological modelling analysis*, Mathematics 11 (2023), 1121.

[8] Bragazzi, N.L., Han, Q., Iyaniwura, S.A., Omame, A., Shausan, A., Wang, X., Woldegerima, W.A., Wu, J. and Kong, J.D. *Adaptive changes in sexual behavior in the high-risk population in response to human monkeypox transmission in Canada can help control the outbreak: insights from a two-group, two-route epidemic model*, J. Med. Virol. 95(4) (2023), e28575.

[9] Brauer, F., Castillo-Chavez, C. and Feng, Z. *Endemic disease models*, in: *Mathematical Models in Epidemiology*, Springer, 2019.

[10] CDC. *About Monkeypox*, 2026. Available at: https://www.cdc.gov/monkeypox/about/index.html

[11] CDC. *FACT SHEET: United States Response to the Clade I Mpox Outbreak in Several African Countries*, 2024. Available at: https://www.cdc.gov/media/releases/2024/s0822-mpox-outbreak.html

[12] CDC. *How Monkeypox Spreads*, 2026. Available at: https://www.cdc.gov/monkeypox/causes/index.html

[13] CDC. *U.S. Case Data: Monkeypox*, 2026. Available at: https://www.cdc.gov/monkeypox/data-research/cases/index.html

[14] Chen, C. and Xiang, Z. *Analysis and optimal control strategies of epidemic models with nonlinear incidence rates*, Adv. Contin. Discrete Models 2025 (2025), 92.

[15] Elmekawy, A., El-Azab, M.S. and El-Shenawy, A. *SIR dengue fever nonlinear mathematical model: a computational framework with numerical simulation*, Nonlinear Sci. 5 (2025), 100073.

[16] Elsonbaty, A., Adel, W., Aldurayhim, A. and El-Mesady, A. *Mathematical modeling and analysis of a novel monkeypox virus spread integrating imperfect vaccination and nonlinear incidence rates*, Ain Shams Eng. J. 15 (2024), 102451.

[17] Fernandes, G.D. and Maldonado, V. *Behavioral aspects and the transmission of monkeypox: a novel approach to determine the probability of transmission for sexually transmissible diseases*, Infect. Dis. Model. 8 (2023), 842–854.

[18] Flores-Pérez, A., González-Olvera, M.A., Chávez-Peña, G., Gallardo-Hernández, A.G. and Torres, L. *Time-delay enhanced SIR model for COVID-19 waves in Mexico: parameter estimation using evolutionary algorithms*, J. Theor. Biol. 613 (2025), 112229.

[19] Janan, T., Fatmawati, Alfiniyah, C., Martini, S., Aldila, D. and Hasan, A. *Dynamical analysis and optimal control of the Mpox transmission model with stratified susceptibility*, Math. Model. Numer. Simul. Appl. 6 (2026), 186–227.

[20] Janan, T., Fatmawati and Hasan, A. *Dynamical Analysis of Mpox Transmission Model Incorporating Asymptomatic Individuals*, Commun. Biomath. Sci. 9 (2026), 48–67.

[21] La Salle, J.P. *The Stability of Dynamical Systems*, SIAM, 1976.

[22] Leandry, L. and Mureithi, E.W. *An investigation on the monkeypox virus dynamics in human and rodent populations for a deterministic mathematical model*, Informatics Med. Unlocked 41 (2023), 101325.

[23] Leicester Mercury. *Rodent pets could be culled after UK monkeypox outbreak*, 2022. Available at: https://www.leicestermercury.co.uk/news/uk-world-news/rodent-pets-could-culled-after-7134597

[24] Li, S., Samreen, Ullah, S., AlQahtani, S.A., Tag, S.M. and Akgül, A. *Mathematical assessment of monkeypox with asymptomatic infection: prediction and optimal control analysis with real data application*, Results Phys. 51 (2023), 106726.

[25] Meetei, M.Z., DarAssi, M.H., Ahmad, I., Khan, M.A., Isa, N.M. and Alzahrani, E. *Mathematical modeling and optimal control analysis of the monkeypox Clade II infection dynamics under the recent cases of USA*, Comput. Ind. Eng. 209 (2025), 111462.

[26] Murray, J.D. *Mathematical Biology: I. An Introduction*, Springer, 2007.

[27] Naidu, D.S. *Optimal Control Systems*, Taylor & Francis, 2002.

[28] Somma, S.A., Akinwande, N.I. and Chado, U.D. *A mathematical model of monkeypox virus transmission dynamics*, Ife J. Sci. 21 (2019), 195–204.

[29] Stephano, M.A., Mayengo, M.M. and Irunde, J.I. *The role of asymptomatic carriers on the dynamics of a lymphatic filariasis model incorporating control strategies*, Results Control Optim. 15 (2024), 100425.

[30] Thornhill, J.P., Barkati, S., Walmsley, S., Rockstroh, J., Antinori, A., Harrison, L.B., Palich, R., Nori, A., Reeves, I. and Habibi, M.S. *Monkeypox virus infection in humans across 16 countries–April-June 2022*, N. Engl. J. Med. 387 (2022), 679–691.

[31] Usman, S. and Adamu, I.I. *Modeling the transmission dynamics of the monkeypox virus infection with treatment and vaccination interventions*, J. Appl. Math. Phys. 5 (2017), 2335–2353.

[32] US. *FACT SHEET: The United States Commitment to Address the Global Mpox Outbreak*, 2024. Available at: https://geneva.usmission.gov/2024/09/25/u-s-commitment-to-address-the-global-mpox-outbreak/

[33] Waseel, F., Streftaris, G., Rudrusamy, B. and Dass, S.C. *Assessing the dynamics and impact of COVID-19 vaccination on disease spread: a data-driven approach*, Infect. Dis. Model. 9(2) (2024), 527–556.

[34] WHO. *Mpox (monkeypox) outbreak 2022*, 2022. Available at: https://www.who.int/emergency/situations/monkeypox-oubreak-2022

[35] WHO. *Mpox*, 2024. Available at: https://www.who.int/news-room/fact-sheets/detail/mpox

[36] WHO. *Mpox*, 2024. Available at: https://www.who.int/news-room/questions-and-answers/item/mpox

[37] WHO. *WHO Director-General declares mpox outbreak a public health emergency of international concern*, 2024. Available at: https://www.who.int/news/item/14-08-2024-who-director-general-declares-mpox-outbreak-a-public-health-\emergency-of-international-concern

[38] Winata, I.G.S., Leonardo, L., Sylfiasari, R., Ekafentie, A., Immanuel, S.S. and Christyani, F. *Unveiling the outcomes of Mpox in pregnancy: a systematic review and single-arm meta-analysis*, Infect. Chemother. 57(1) (2025), 119–130.

[39] Wireko, F.A., Adu, I.K., Sebil, C. and Asamoah, J.K.K. *A fractal-fractional order model for exploring the dynamics of monkeypox disease*, Decis. Anal. J. 8 (2023), 100300.

[40] Xu, T., Zhang, J. and Jin, Z. *Analysis of final size and peak time for SIR epidemic model on simplicial complexes*, Chaos Solitons Fractals 196 (2025), 116390.

[41] Yapışkan, D., Yurtoğlu, M., Avcı, D., İskender Eroğlu, B.B. and Bonyah, E. *A novel model for monkeypox disease: system analysis and optimal preventive strategies*, Iran. J. Sci. 47 (2023), 1665–1677.

[42] Zhang, X.S., Mandal, S., Mohammed, H., Turner, C., Florence, I., Walker, J., Niyomsri, S., Amirthalingam, G., Ramsay, M., Charlett, A. and Vickerman, P. *Transmission dynamics and effect of control measures on the 2022 outbreak of Mpox among gay, bisexual, and other men who have sex with men in England: a mathematical modelling study*, Lancet Infect. Dis. 24(1) (2024), 65–74.